

# Modifying the Electrical Properties of $\text{Ba}_{0.85}\text{Ca}_{0.15}\text{Zr}_{0.1}\text{Ti}_{0.9}\text{O}_3$ Ceramics by the Nanocrystals-Induced Method

Piewpan Parjansri<sup>1</sup>, Manlika Kamnoy<sup>2</sup>, Uraiwan Intatha<sup>3</sup>, and Sukum Eitsayeam<sup>2,\*</sup>

<sup>1</sup>Physics Division, Faculty of Science and Technology, Rajamangala University of Technology Krungthep, Bangkok 10120, Thailand

<sup>2</sup>Department of Physics and Materials Science, Faculty of Science, Chiang Mai University, Chiang Mai 50200, Thailand

<sup>3</sup>School of Science, Mae FahLuang University, 57100 Chiang Rai, Thailand

This work investigated the phase formation and electrical properties of  $\text{Ba}_{0.85}\text{Ca}_{0.15}\text{Zr}_{0.1}\text{Ti}_{0.9}\text{O}_3$  (BCZT) prepared by the nanocrystals-induced method. We prepared the nanocrystals or seeds by the molten salt method, using  $\text{CaCO}_3$  and  $\text{TiO}_2$  oxides as starting materials. The  $\text{CaTiO}_3$  seeds showed a pure perovskite phase, and we obtained a particle size of  $\sim 300$  nm. After that, we mixed the CT seed with the starting powders of  $\text{Ba}_{0.85}\text{Ca}_{0.15}\text{Zr}_{0.1}\text{Ti}_{0.9}\text{O}_3$  ceramic, prepared by the solid state reaction method. Results found that all ceramics showed a pure perovskite phase. The density values were in the range of 5.51 to 5.64  $\text{g/cm}^3$ , while relative density values were 96–99%. We measured the electrical properties (including dielectric, ferroelectric, and piezoelectric properties) as a function of  $\text{CaTiO}_3$  seed content. We obtained the highest dielectric constant ( $\epsilon_r \sim 4239$ ) and lowest dielectric loss ( $\tan \delta \sim 0.010$ ) measured at room temperature from a sample with  $x = 0.08$ . Moreover, the BCZT doped with  $\text{CaTiO}_3$  seed ( $x = 0.10$ ) showed the highest values for the piezoelectric charge coefficient ( $d_{33} \sim 477$  pC/N, piezoelectric voltage coefficient ( $g_{33} \sim 16 \times 10^{-3}$  Vm/N, and thickness mode electromechanical coupling ( $k_t \sim 51.18\%$ ). Results suggested that  $\text{CaTiO}_3$ -seeds enhanced the electrical properties of the BCZT ceramic using low calcination temperatures and with less dwelling time.

**Keywords:** Molten Salt Method, Seed-Induced Method, Perovskite Phase, Piezoelectric Properties.

## 1. INTRODUCTION

Barium titanate ( $\text{BaTiO}_3$ ; BT) was the first useful lead-free piezoelectric ceramic, and still receives considerable attention because of its very high dielectric constant, making it an excellent material for use as a capacitor.<sup>1</sup> However, this ceramic exhibits poor piezoelectric properties. Many researchers have studied and reported on the fabrication and characterization of BT-based ceramics by various methods. The various ion substitutions in the A and B sites of the  $\text{BaTiO}_3$  ceramic structure represent one of the methods to enhance the electrical properties of those ceramics. Researchers have studied the modification of BT ceramic by the addition of calcium (Ca) into the Ba site (A-site) and zirconium (Zr) into the Ti site (B-site).<sup>2</sup> The  $\text{Ba}_{0.85}\text{Ca}_{0.15}\text{Zr}_{0.1}\text{Ti}_{0.9}\text{O}_3$  ceramic system serves as one of

the modified BT ceramics to receive considerable attention because of its high piezoelectric and dielectric properties. Liu and Ren have reported the  $\text{Ba}_{0.85}\text{Ca}_{0.15}\text{Zr}_{0.1}\text{Ti}_{0.9}\text{O}_3$  ceramic with a high  $d_{33}$  value of  $\sim 600$  pC/N.<sup>3</sup>

However, we obtained the highest  $d_{33}$  value using high calcination temperatures, sintering temperatures, and dwelling times. Researchers have reported different procedures capable of reducing the calcination temperature, while also improving the electrical properties of piezoelectric ceramics. Researchers have widely studied the doping of various metal oxides in BT-based and BCZT ceramics, due to their resultant lower calcination temperatures and improved piezoelectric properties.<sup>4–6</sup> Recently, researchers have reported a new methodology to reduce calcination temperatures by using the seed-induced method and template grain growth (TGG) method. Researchers well-know that the seeding and template process in ceramics helps to

\*Author to whom correspondence should be addressed.

develop a single crystal growth under controlled temperature conditions, observing good electrical properties.<sup>7–9</sup> Li et al. reported the perovskite phase formation and electrical properties of  $\text{Pb}(\text{Zn}_{1/3}\text{Ta}_{2/3})\text{O}_3$  ceramic, prepared using  $\text{PbTiO}_3$  as seeds, finding that a pure perovskite phase could be formed at low calcination temperatures, while obtaining a high dielectric constant ( $\epsilon_r$ ) and low dielectric loss ( $\tan \delta$ ) for the seed-added sample.<sup>8</sup> Ye et al. have reported the template grain growth method,<sup>9</sup> studying the effect of  $\text{BaTiO}_3$  (BT) template on the electrical properties of  $\text{Ba}_{0.85}\text{Ca}_{0.15}\text{Zr}_{0.10}\text{Ti}_{0.90}\text{O}_3$ . Preparing the BT-template by the molten-salt method and using a calcination temperature of 1100 °C, these researchers found that the textured BCZT ceramics (templates-added sample) showed a piezoelectric coefficient of  $d_{33} \sim 470$  pC/N, an electromechanical coefficient of  $k_p \sim 40\%$ , and a Curie temperature ( $T_C$ ) higher than the sample without BT templates. The above literature suggests that the seed-induced method and template grain growth can enhance the electrical properties of piezoelectric ceramics using a low calcination temperature.

In the present work, we prepared and characterized  $\text{Ba}_{0.85}\text{Ca}_{0.15}\text{Zr}_{0.1}\text{Ti}_{0.9}\text{O}_3$  ceramics using the seed-induced method. We used  $\text{CaTiO}_3$  (CT) prepared by the molten-salt method as seeds, because it exhibits different structures depending on the transition temperature and shows an orthorhombic phase at room temperature.<sup>10</sup> However, we obtained the perovskite structure of CT powder from a preparation by a mixed oxide method using a high calcination temperature of about 1350 °C.<sup>11</sup> Thus, we used nano-size particles of CT powder prepared by the molten salt method as seed for producing the pure perovskite phase, controlling the grain orientation and crystal orientation direction and improving the electrical properties for the BCZT ceramics.

## 2. EXPERIMENTAL DETAILS

We synthesized the  $\text{Ba}_{0.85}\text{Ca}_{0.15}\text{Zr}_{0.1}\text{Ti}_{0.9}\text{O}_3$  ceramic samples using the seed-induced method. We prepared the seed via the molten salt method, using  $\text{CaCO}_3$  and  $\text{TiO}_2$  oxides as starting materials. We mixed the starting powder by ball-milling for 24 h, mixed with KCl–NaCl salt (1:1) for 30 min, then heated at 900 °C for 2 h. Then, we washed them with hot deionized water several times until finding no trace of anion. After that, we mixed the CT seed with the starting material of the BCZT system, prepared by the mixed oxide method. We mixed stoichiometric amounts of  $\text{BaCO}_3$  (99%, Sigma–Aldrich),  $\text{CaCO}_3$  (98.5–100.5%, Sigma–Aldrich),  $\text{ZrO}_2$  (99%, Sigma–Aldrich),  $\text{TiO}_2$  (99–105.5%, Sigma–Aldrich),  $\text{Nb}_2\text{O}_5$  (99%, Sigma–Aldrich), and CT seeds. We varied the CT seed content from 0.0 to 10.0 mol% ( $x = 0.0, 0.04, 0.08, \text{ and } 0.10$ ). We ball-milled the mixed powder for 24 h using ethanol as a solvent with zirconia grinding media, then dried in an oven at 120 °C. We calcined all ceramic powders at 1250 °C for 2 h. Then, we pressed the calcined powder into a disk shape of

thickness and diameter about 2.0 mm and 10 mm, respectively; afterwards, we sintered them at 1450 °C for 4 h. We investigated the phase formation and microstructure of the samples by X-ray diffraction (XRD) (XRD 6000, Shimadzu) and scanning electron microscopy (SEM). For electrical properties characterization, we polished the sintered ceramics, and we coated both faces with silver as electrodes. We investigated the dielectric properties of the sintered ceramics as a function of frequency and temperature by using an automated dielectric measurement system (E4980A Precision LCR meter). The coated samples had an applied electric field of 1–2 kV/mm for measuring ferroelectric properties by using a Sawyer Tower circuit. We poled the specimens by applying a DC field of 3 kV/mm for 30 min in a silicone oil bath at 28 °C. After 24 h, we measured the piezoelectric charge coefficient ( $d_{33}$ ) by using a S5865  $d_{33}$  meter (KCF Technologies). Moreover, we calculated the piezoelectric voltage coefficient ( $g_{33}$ ) and the electromechanical coupling coefficients ( $k_t$ ), plotted as a function of the CT seed content

## 3. RESULTS AND DISCUSSION

From the introduction section, many researchers have carried out studies on developing lead-free piezoelectric ceramics to replace the PZT-based ceramics in piezoelectric applications.

$\text{Ba}_{0.85}\text{Ca}_{0.15}\text{Zr}_{0.1}\text{Ti}_{0.9}\text{O}_3$  ceramic represents one of the materials of interest, displaying the highest  $d_{33}$  value. However, some electrical properties (e.g.,  $\epsilon_r$ ,  $\tan \delta$ , and  $T_C$ ) still cannot compare with PZT-based ceramics. Also, we obtained the highest  $d_{33}$  value at the highest calcination temperature, using very long dwelling times. The modification of crystal structure by controlling the grain orientation serves as a well-known method to enhance the properties and performance of piezoelectric materials. In this research, we used the seed-induced method. We successfully obtained BCZT ceramics, prepared using the CT seed-induced method. We investigated the phase structure, microstructure, and the electrical properties. We synthesized the CT seed powder by the molten-salt method. The phase formation of the CT seed presented that we obtained pure perovskite with a small particle size of about  $\sim 300$  nm, by using heating temperatures of 900 °C for 2 h. We indexed the pure perovskite phase of the CT seed in reference to the orthorhombic structure of  $\text{CaTiO}_3$  (JCPDS No. 01-086-1393), confirmed from XRD patterns, as shown in Figure 1. Inset (a) in Figure 1 shows the microstructure of the CT seed powder. We mixed the CT seed obtained with the metal oxides of BCZT systems by the mixed oxide method. The results showed that the non-seed sample and CT seed-added sample possessed a pure perovskite phase, as displayed in Figure 2. For the expanded graph of XRD patterns around  $2\theta$  of 44–46°, the non-seed sample and seed-added samples showed a broad peak and sharp

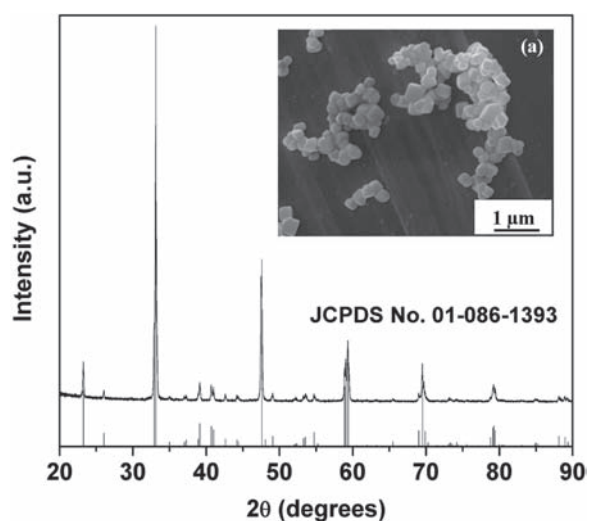


**Figure 1.** XRD patterns and SEM micrograph of  $\text{CaTiO}_3$ -seed powder heated at  $900^\circ\text{C}$  for 2 h.

peaks, respectively. The peaks sharpness suggested an increase in the crystallite size of the BCZT ceramics. The XRD spectra suggested that the CT-seed changed the phase structure of BCZT ceramics from the co-existence of rhombohedral-orthorhombic to orthorhombic phase.<sup>12</sup> Figure 3 illustrates the SEM micrographs of BCZT-CT seed ceramics sintered at  $1450^\circ\text{C}$  for 4 h, showing a more homogeneous and uniform grain for the CT-seed BCZT for  $x = 0.04$  and  $x = 0.10$  than the non-CT seed sample. Conversely, we found the melting grain boundary for the sample with  $x = 0.08$ . This result suggested that the grain growth occurred close to the end.

Increasing CT seed content to  $x = 0.10$  gave an effect of the appearance of pores. Table I lists the grain sizes and densities of all samples. The grain size tended to increase with increasing CT seed content from  $x = 0.00$ – $0.08$ , then decreased for the  $x = 0.10$  sample. The decreasing grain

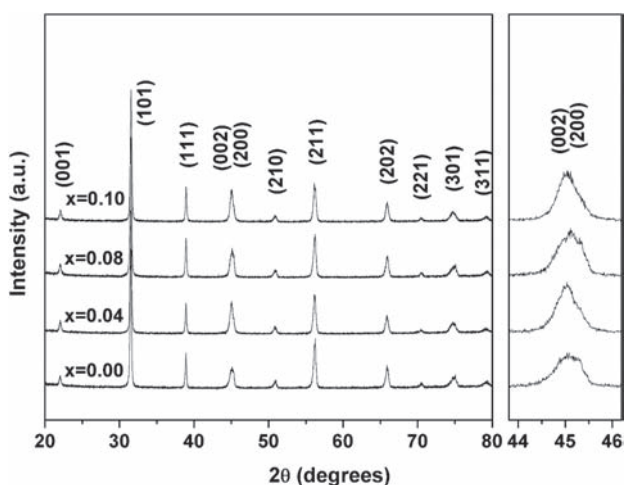


**Figure 2.** XRD patterns of BCZT-CT seed ceramics sintered at  $1450^\circ\text{C}$  for 4 h.

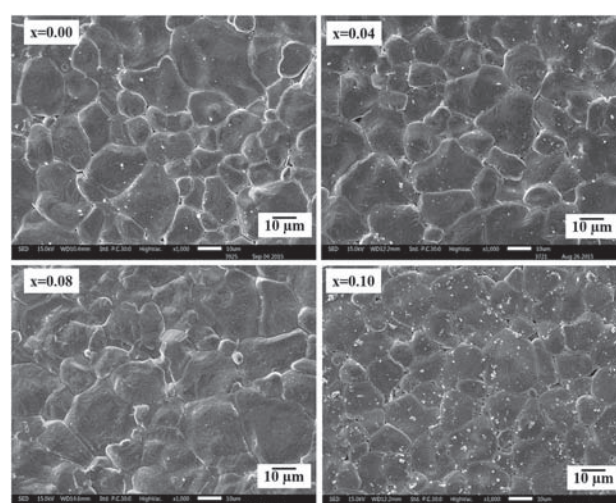


**Figure 3.** SEM micrographs of sintered BCZT-CT seed surface.

size may be due to the excess CT particles accumulating near the grain boundaries, leading to grain growth being interrupted during the sintering process.<sup>13,14</sup> The density values of the samples for  $x = 0.08$  and  $x = 0.10$  showed the highest value (with 99% of theoretical density) and the lowest value, respectively, relating to the SEM micrographs. Figure 4 illustrates the dielectric constant ( $\epsilon_r$ ) and dielectric loss ( $\tan \delta$ ) as a function of frequency measured at room temperature for the BCZT-CT seed ceramics. We observed that the CT seed had an effect on the dielectric properties of the BCZT ceramic.  $\epsilon_r$  showed little change with frequency for all samples, while we found the highest value for the sample with  $x = 0.08$ . The highest  $\epsilon_r$  may have resulted from the dense ceramic, which related to the density value.<sup>15</sup> The  $\tan \delta$  of all ceramics showed significant changes with increasing frequency and CT seed content, because the concentration of charge carriers was not constant.<sup>16</sup> Table I lists the value of  $\epsilon_r$  and  $\tan \delta$ . The results indicated that adding CT seed enhanced the maximum value of  $\epsilon_r \sim 4239$  and the lowest of  $\tan \delta \sim 0.01$ .

The dielectric properties analyzed as a function of temperature in a range from  $30^\circ\text{C}$  to  $250^\circ\text{C}$  are shown in Figure 5. Figure 5(a) displays the dielectric constant ( $\epsilon_r$ ) and dielectric loss ( $\tan \delta$ ), with temperature measured at 1 kHz for all samples. Figure 5(b) shows the frequency and temperature dependence of the dielectric constant ( $\epsilon_r$ ). We observed that all ceramic samples showed a normal ferroelectric behavior, confirmed by the maximum dielectric constant peak. Researchers well-know that ferroelectric behavior (relaxor and normal ferroelectric) can be described from dielectric properties as a function of temperature. In the case of relaxor ferroelectric behavior, the dielectric constant at maximum peak showed a broader peak and strong frequency dependence. For the normal ferroelectric, the dielectric constant had a weak dependence on frequency and also a sharp dielectric peak.<sup>17</sup> The above mentioned theory considers that the CT seed additions

**Table I.** Density, grain size and dielectric properties of ceramic samples.

| Samples | Density (g/cm <sup>3</sup> ) | GS ( $\mu\text{m}$ ) | % Relative density | Dielectric ( $\epsilon_r$ ) | Loss (tan $\delta$ ) | Dielectric <sup>a</sup> ( $\epsilon_r$ ) | Loss <sup>a</sup> (tan $\delta$ ) | $T_c$ ( $^\circ\text{C}$ ) |
|---------|------------------------------|----------------------|--------------------|-----------------------------|----------------------|--|-----------------------------------|----------------------------|
| 0.00    | 5.5964                       | 13.50                | 96.8               | 3672                        | 0.0139               | 10939                                    | 0.0104                            | 100.24                     |
| 0.04    | 5.5632                       | 14.29                | 97.3               | 3594                        | 0.0128               | 10177                                    | 0.0096                            | 100.15                     |
| 0.08    | 5.6415                       | 15.69                | 99.0               | 4239                        | 0.0106               | 9653                                     | 0.0095                            | 84.98                      |
| 0.10    | 5.5099                       | 13.40                | 98.0               | 3362                        | 0.0142               | 10191                                    | 0.0100                            | 95.67                      |

Note: <sup>a</sup>Dielectric properties at  $T_c$  temperature.

have no effect on the BCZT ceramic structure. The dielectric constant ( $\epsilon_r$ ) at the maximum peak or the phase transition point (Curie temperature;  $T_c$ ) tended to decrease with increasing CT seed content from  $x = 0.0$  to  $x = 0.08$ , then increased for the sample with  $x = 0.10$ .

The  $\epsilon_r$  of the ceramics showed a value in the range of 9653–10936. The decreasing  $\epsilon_r$  might have resulted from the decreased dielectric polarization rotation. The addition of CT seed in the BCZT ceramic may result in a decrease of dielectric polarization.<sup>18</sup> As we well-know, the dielectric properties depend on the microstructure of the ceramic, especially the grain size and grain morphology (homogenous grain). The dielectric constant of a ceramic strongly depends on the domain wall mobility.<sup>18</sup> Moreover, the change of dielectric constant may result from the internal stress that occurs at the phase transition temperature. The uniform and homogenous grain of ceramics generates less internal stress of the lattice, leading to an easier movement of the domain wall.<sup>18</sup> We can notice that the dielectric properties in the present work can be described by the above mentioned theory; as for the sample with  $x = 0.08$ , the dielectric at  $T_c$  decreased potentially because the grain of the ceramic was not uniform.

Dielectric loss (tan  $\delta$ ) was little changed in a temperature range from 30  $^\circ\text{C}$  to 200  $^\circ\text{C}$ , with values less than 0.01 for all samples, then tending to increase at higher temperatures. The phase transition temperature

(Curie temperature;  $T_c$ ) shifted slightly toward a lower temperature with increasing CT seed content. The Curie temperature ( $T_c$ ) decreased potentially due to the random substitution of CT seed particles, leading to the deformation of the  $\text{ABO}_3$  lattice.<sup>3,19</sup> Figure 6 plots the ferroelectric loop and parameters of the ferroelectric loop for the BCZT-CT seed ceramics. From Figure 6, we found that the Polarization ( $P$ ) versus electric field ( $E$ ) showed a gradual change with CT seed content, as shown in Figure 6(a). All samples showed slim  $P$ - $E$  loops, typical for normal ferroelectric hysteresis. The inset in Figure 6(a) expands the polarization of the samples. Figure 6(b) presents plots of the remnant polarization ( $P_r$ ) and coercive field ( $E_c$ )

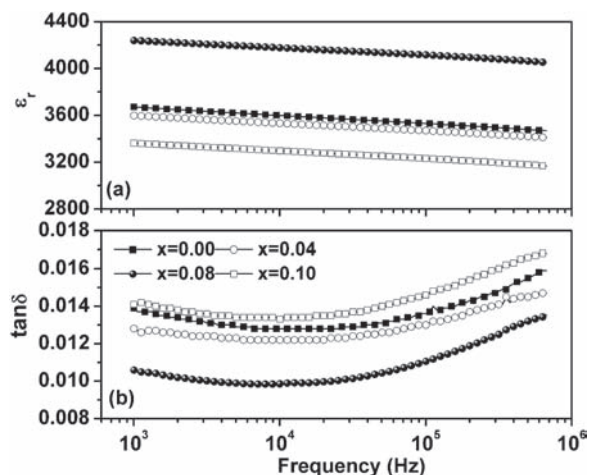


**Figure 4.** Frequency dependence of dielectric constant,  $\epsilon_r$  (a) and dielectric loss, tan $\delta$  (b) for BCZT-CT seed ceramics.

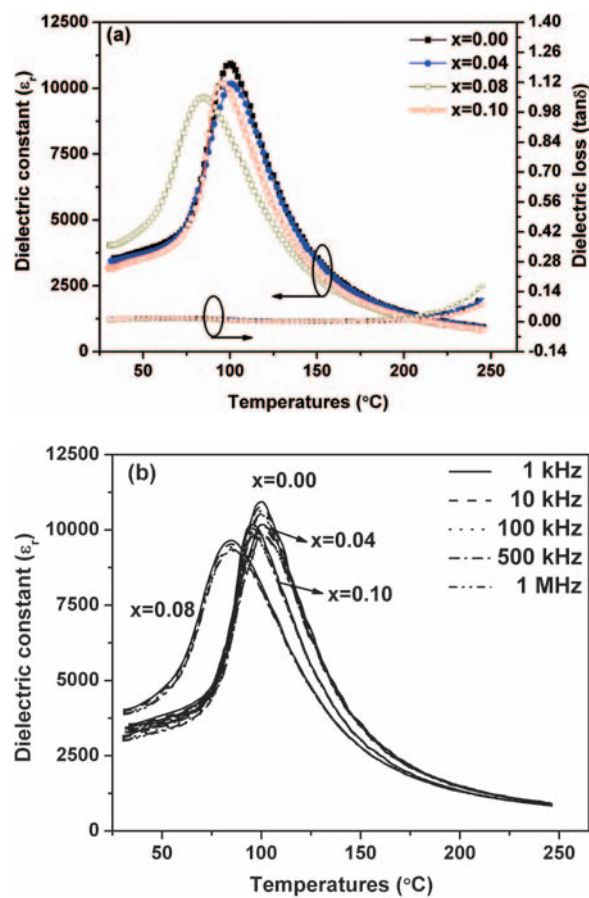


**Figure 5.** (a) Dielectric constant ( $\epsilon_r$ ) and dielectric loss (tan $\delta$ ) as a function of temperature at 1 kHz and (b) dielectric constant ( $\epsilon_r$ ) with frequency for BCZT-CT seed ceramics.

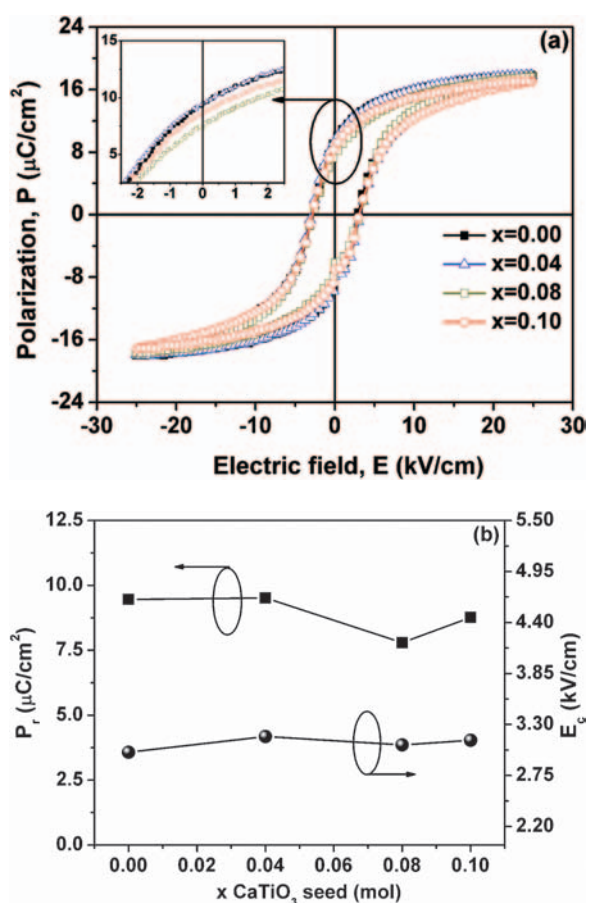


**Figure 6.** (a) Ferroelectric loops and (b) remnant polarization ( $P_r$ ) and coercive field ( $E_c$ ) analyzed at room temperature.

of the BCZT-CT seed ceramics. The results indicated that the  $P_r$  and  $E_c$  values had little change with CT seed. The  $P_r$  values of the ceramics were in the range of 7.79–9.52  $\mu\text{C}/\text{cm}^2$ , and we obtained the highest value for the  $x = 0.04$  sample (as listed in Table II).

The decreasing  $P_r$  values for samples with  $x = 0.08$  may have been due to the increase of inner stress with higher CT seed addition, being related to the SEM micrograph showing grain boundary mobility and the achievable domain alignment decreased.<sup>20</sup> The higher  $P_r$  value for samples of  $x = 0.00$ – $0.04$  and  $x = 0.10$  was due to the uniform and homogeneous grains leading to the easier reorientation and polarization switching of the domain walls during the electric field cycle.<sup>21,22</sup>

**Table II.** Ferroelectric, piezoelectric and electromechanical properties of BCZT-CT seed ceramics.

| Samples | $P_r$<br>( $\mu\text{C}/\text{cm}^2$ ) | $E_c$<br>(kV/cm) | $d_{33}$<br>(pC/N) | $g_{33}$<br>( $10^{-3}$ Vm/N) | $k_t$<br>(%) |
|---------|--|------------------|--------------------|-------------------------------|--------------|
| 0.00    | 9.46                                   | 3.00             | 474                | 14.58                         | 50.51        |
| 0.04    | 9.52                                   | 3.17             | 435                | 13.67                         | 50.51        |
| 0.08    | 7.79                                   | 3.13             | 424                | 11.30                         | 40.83        |
| 0.10    | 8.77                                   | 3.13             | 477                | 16.02                         | 51.18        |

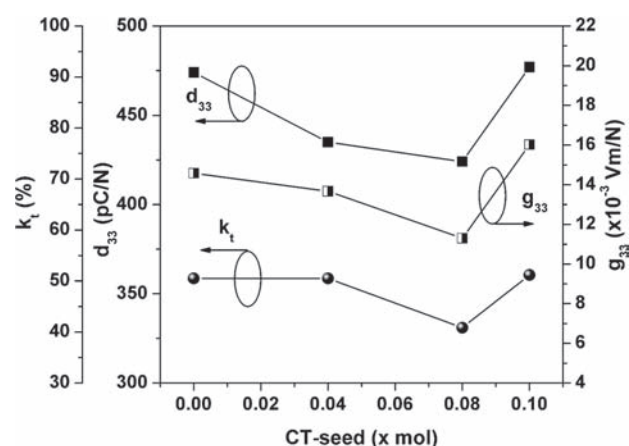


**Figure 7.** Piezoelectric charge coefficient ( $d_{33}$ ), piezo-electric voltage coefficient ( $g_{33}$ ) and thickness electromechanical coupling ( $k_t$ ) for BCZT-CT ceramic.

For the characterization of piezoelectric and electromechanical properties, we poled the electrode specimen at room temperature by applying an electrical field of 3 kV/mm for 30 min. We then left it at room temperature for 24 h before measuring their piezoelectric coefficient ( $d_{33}$ ). Figure 7 illustrates the piezoelectric coefficient ( $d_{33}$ ), piezoelectric voltage ( $g_{33}$ ) coefficient, and thickness mode electromechanical coupling ( $k_t$ ) of the BCZT-CT seed ceramics. The results found that the  $d_{33}$ ,  $g_{33}$ , and  $k_t$  values showed similar behavior. Table II lists the values of  $d_{33}$ ,  $k_t$ , and  $g_{33}$ . From the data, we saw that as the CT seed content increased from  $x = 0.00$  to  $x = 0.08$ , the values tended to clearly decrease, then slightly increase for samples with  $x = 0.10$ . The highest  $d_{33}$  and  $k_t$  values were 477 and 51.18, respectively, found for the sample of CT seed ( $x = 0.10$ ). The increasing  $d_{33}$  and  $k_t$  for the samples with  $x = 0.10$  related to the uniform grain that resulted in the domain wall movement, making domain reorientation easier during the poling process.<sup>22–25</sup> The piezoelectric properties were dependent on the domain wall motion, while domain wall motion was dependent on the dopant (CT seed adding). On the other hand, the decreasing  $d_{33}$  and  $k_t$  values for the sample of  $x = 0.08$  may have resulted from the decreasing  $P_r$ , leading to the polarization switching being decreased. We determined the  $g_{33}$  value by using expression (1):<sup>26</sup>

$$g_{33} = \frac{d_{33}}{\epsilon_0 \epsilon_r} \quad (1)$$

where  $\epsilon_0$  was permittivity of a free space, and  $\epsilon_r$  was relative permittivity. The  $g_{33}$  values were in the range of  $1.30 \times 10^{-3}$  to  $16.02 \times 10^{-3}$  Vm/N. We obtained the highest  $g_{33}$  value for the sample with CT seed of  $x = 0.10$ . The above results showed that the seed-induced method using  $\text{CaTiO}_3$  as seed had a significant influence on the electrical properties of the BCZT ceramic, by controlling the grain growth and reducing the temperature for phase formation.

We should note that these ceramic can replace PZT-based materials, being suitable for electronic device applications.

#### 4. CONCLUSION

We investigated the effect of CT nanocrystals or CT seed on the electrical properties of BCZT ceramics. We found that all ceramics showed a pure perovskite phase. Highest density, relative density, grain size, and  $\epsilon_r$  values were 5.64 g/cm<sup>3</sup>, 99%, 15.69, and 4239, respectively, obtained for CT seed-added with  $x = 0.08$ . Tan  $\delta$  values were lower than 0.02 for all samples. We obtained the highest values of  $d_{33} \sim 477$  pC/N,  $g_{33} \sim 16 \times 10^{-3}$  Vm/N, and  $k_t \sim 51.18\%$  for the sample with  $x = 0.10$ . We can conclude that the CT seed helped to improve the electrical properties of the BCZT ceramics.

**Acknowledgment:** The authors would like to thank the Department of Physics and Materials Science, Faculty of Science at Chiang Mai University, the National Research University Project under Thailand's Office of the High Education Commission, Science and Technology Research Institute, Chiang Mai University for financial support.

#### References and Notes

1. D. Berlincourt and H. Jaffe, *Phys. Rev.* 111, 143 (1958).
2. O. P. Thakur, C. Prakash, and A. R. James, *J. Alloy. Comp.* 470, 548 (2009).
3. W. Liu and X. Ren, *Phys. Rev. Lett.* 103, 257602 (2009).
4. Z. Dai and Y. Akishige, *Funct. Mater. Lett.* 7, 1350074 (2014).
5. J. Wu, D. Xiao, W. Wu, Q. Chen, J. Zhu, Z. Yang, and J. Wang, *Scripta Mater.* 65, 771 (2011).
6. Y. Cui, C. Yuan, X. Liu, X. Zhao, and X. Shan, *J. Mater. Sci.: Mater. Electron.* 24, 654 (2013).
7. C. Duran, S. T. McKinstry, and G. L. Messing, *J. Am. Ceram. Soc.* 83, 2203 (2000).
8. Z. Li, A. Wu, and P. M. Vilarinho, *Chem. Mater.* 16, 717 (2004).
9. S. K. Ye, J. Y. Fuh, and L. Lu, *Appl. Phys. Lett.* 100, 252906 (2012).
10. Y. J. Wong, J. Hassan, and M. Hashim, *J. Alloy. Comp.* 571, 138 (2013).
11. H. F. Kay and P. C. Bailey, *Acta. Cryst.* 10, 219 (1957).
12. C. K. I. Tan, S. Shannigrahi, K. Yao, and J. Ma, *J. Electroceram.* 35, 19 (2015).
13. R. B. Atkin and R. M. Fulrath, *J. Am. Ceram. Soc.* 54, 265 (1971).
14. M. N. Rahaman, *Ceramics Processing and Sintering*, Marcel Dekker, New York (1995), pp. 476–482.
15. A. Banerjee, A. Bandyopadhyay, and S. Bose, *J. Am. Ceram. Soc.* 89, 1594 (2006).
16. U. Intatha, S. Eitssyeam, J. Wang, and T. Tunkasiri, *Curr. Appl. Phys.* 10, 21 (2010).
17. L. E. Cross, *Ferroelectrics* 76, 241 (1987).
18. V. R. Mudinepalli, L. Feng, W.-C. Lin, and B. S. Murty, *J. Adv. Ceram.* 4, 46 (2015).
19. D. Shan, Y. Qu, and J. Song, *J. Mater. Res.* 22, 730 (2007).
20. J. Ma, X. Liu, M. Jiang, H. Yang, G. Chen, X. Liu, L. Qin, and C. Luo, *J. Mater. Sci.: Mater. Electron.* 25, 992 (2014).
21. J. H. Park, B. K. Kim, K. H. Song, and S. J. Park, *J. Mater. Sci. Mater. Electron.* 6, 97 (1995).
22. K. Kumar and B. Kumar, *Ceram. Int.* 38, 1157 (2012).
23. C. A. Randall, N. Kim, J. P. Kucera, W. W. Cao, and T. R. Shrout, *J. Am. Ceram. Soc.* 81, 677 (1998).
24. S. Zhang, R. Xia, T. R. Shrout, G. Zang, and J. Wang, *J. Appl. Phys.* 100, 104108 (2006).
25. M. Demartin and D. Damjanovic, *Appl. Phys. Lett.* 68, 3046 (1996).
26. A. J. Moulson and J. M. Herbert, *Electroceramics Materials, Properties, Applications*, 2nd edn., Wiley and Sons, New York (2003).

Received: 30 December 2015. Accepted: 29 June 2016.